Schweizerische Eidgenossenschaft
Confédération suisse
Confederazione Svizzera
Confederaziun svizra

Federal Department of the Environment, Transport, Energy and Communications DETEC

Swiss Federal Office of Energy SFOE
Energy Research and Cleantech Division

REEL Demo – Romande Energie ELectric network in local balance Demonstrator

Deliverable: 4d Validation of an Advanced Control Algorithm based on Short-term Forecasting of PV Generation

Demo site: Aigle

Developed by
Rahul Gupta and Prof. Dr. Mario Paolone
Distributed Electrical Systems Laboratory, EPFL

[Lausanne, 29.05.2022]

NOTE: This work is under review for the publication in the IEEE Open Access Journal of Power and Energy. The paper under review is titled as "Reliable Dispatch of Active Distribution Networks via a Two-layer Grid-Aware Model Predictive Control". The article is attached at the end of the deliverable.

1 Description of deliverable and goal

1.1 Executive summary

Dispatching active distribution networks (ADNs) is an energy-intensive application that, if implemented via Battery Energy Storage Systems (BESSs), may require large capacity of these assets to fully balance the uncertainties caused by the stochastic demand and generation. Insufficient BESSs capacity often leads to their State-of-charge (SOC) saturation resulting in unreliable dispatch tracking.

This work proposes, and experimentally validates, a real-time control scheme that achieves a highly-reliable dispatching of ADNs while ensuring that BESSs SOC is not saturated during the daily operation. The proposed scheme uses a two-layer model predictive control (MPC). The *upper layer* MPC, running every 5-minutes, optimizes BESSs SOC trajectories while minimizing the tracking error considering the prosumption forecast of the whole day. Then, the *lower layer* MPC, running every 30 seconds, takes BESSs SOC trajectories as constraints while achieving a high-resolution tracking of the dispatch plan over the current 5-minutes time horizon. Both layers account for the grid constraints using the Augmented Relaxed Optimal Power Flow (AR-OPF) model, an exact convex relaxation of the original AC-OPF, used in this paper for the first time in the literature to solve a real-time constrained control problem for ADNs.

Both the layers are supported by day-ahead and intra-day forecasts of the uncontrollable injections such as demand, PV and Hydro generation. The proposed framework is experimentally validated using a 1.5 MVA/2.5 MWh BESS connected to an actual 24-node medium voltage (MV) ADNs in Aigle, Switzerland hosting uncontrollable 3.2 MWp distributed photovoltaic generation, 3.4 MVA hydro generations, and 2.8 MW base demand. The RT control problem is formulated as a Model Predictive Control (MPC) that computes the active and reactive power setpoints of the battery energy storage system BESS such that it tracks the dispatch plan at the GCP while obeying the grid and the BESS constraints.

1.2 Research question

Can we enhance the dispatching performance using short-term forecast of uncontrollable PV and demand?

1.3 Novelty of the proposed solutions compared to the state-of-art

The main contributions of this work are listed below.

- Development of a two-layer model predictive control of BESS for achieving dispatch of a power distribution network while ensuring that BESS is not saturated.
- Development of day-ahead and intra-day forecast algorithms.
- Validation of the dominant model in a full-scale real environment via the REeL demonstrator site in Aigle, Switzerland.

1.4 Methodology description

We refer to attached pre-print article below [1] for description on the methodology and experimental results.

Reliable Dispatch of Active Distribution Networks via a Two-layer Grid-Aware Model Predictive Control

Rahul Gupta, Antonio Zecchino, Ji-Hyun Yi, Mario Paolone

***Abstract*—Dispatching active distribution networks (ADNs) is an energy-intensive application that, if implemented via Battery Energy Storage Systems (BESSs), may require large capacity of these assets to fully balance the uncertainties caused by the stochastic demand and generation. Insufficient BESSs capacity often leads to their State-of-charge (SOC) saturation resulting in unreliable dispatch tracking. This work proposes, and experimentally validates, a real-time control scheme that achieves a highly-reliable dispatching of ADNs while ensuring that BESSs SOC is not saturated during the daily operation. The proposed scheme uses a two-layer model predictive control (MPC). The *upper layer* MPC, running every 5-minutes, optimizes BESSs SOC trajectories while minimizing the tracking error considering the prosumption forecast of the whole day. Then, the *lower layer* MPC, running every 30 seconds, takes BESSs SOC trajectories as constraints while achieving a high-resolution tracking of the dispatch plan over the current 5-minutes time horizon. Both layers account for the grid constraints using the Augmented Relaxed Optimal Power Flow (AR-OPF) model, an exact convex relaxation of the original AC-OPF, used in this paper for the first time in the literature to solve a real-time constrained control problem for ADNs. The proposed framework is experimentally validated using a 1.5 MVA/2.5 MWh BESS connected to an actual 24-node medium voltage (MV) ADNs in Aigle, Switzerland hosting uncontrollable 3.2 MWp distributed photovoltaic generation, 3.4 MVA hydro generations, and 2.8 MW base demand.**

***Index Terms*—Active distribution networks, dispatching, model predictive control, battery, AC optimal power flow.**

I. Introduction

Increasing the displacement of conventional power generation towards stochastic renewable (e.g., [1], [2]) is causing increased power imbalances leading to increased reserve requirements in power transmission grids (e.g., [3], [4]). At the same time, such a displacement is at the origin of operational issues in power distribution systems associated to the delivered quality-of-service (mainly associated to voltage quality and its control) as well as lines and transformers congestion [5], [6]).

Dispatching power distribution networks has been proposed in the existing literature as a way to tackle the problem of bulk transmission systems imbalances at the local scale and, at the same time, solve local distribution grid operational issues (e.g., [7], [8]). This process is achieved by controlling suitable distributed energy resources (DERs) in order to indirectly regulate the power injections of heterogeneous and stochastic resources according to a pre-defined power trajectory established the day before operation [9], [10]. In these schemes, distribution system operators (DSOs) may determine the day before operation their *dispatch plan* by taking into account uncertainties of stochastic power injections and follow it during the day of operation by controlling flexible resources such as battery energy storage systems (BESSs). Different dispatching frameworks have been already proposed by the Authors of this paper. For example, the work in [9] proposed and validated a dispatching framework on an medium voltage (MV) feeder using a utility-scale BESS. The work in [11] proposed and validated a day-ahead dispatching framework on a micro-grid using multiple controllable DERs. Both controls were formulated to track the dispatch plan over a short horizon (i.e., 5 minutes) with the consequence for the control to be myopic with respect to prosumers' uncertainties in the forthcoming timesteps during the rest of the day. The consequence is that early saturation of the flexibility offered by controllable resources (e.g., BESSs State-of-Charge - SOC) may occur, hence interrupting the reliable tracking of the dispatch plan. A way to solve the problem has been proposed in [11] by optimally curtailing the excess of power from renewable stochastic generation. Another solution is to increase the time-ahead horizon period (e.g., [12]) in the real-time (RT) MPC of the schemes proposed in [9], [11]. However, this approach increases the computation time (due to large number of variables) and may exceed the real-time actuation time deadline of the MPC controller. Additionally, when the above schemes are implemented on a grid with rich stochastic injections, a successful dispatch requires a large BESS capacity, which might be challenging to be procured by the DSOs due to regulatory constraints and (sufficiently low) payback times. Furthermore, the works in [9], [12] did not account for the grid constraints and the work in [11] did consider the grid constraints via a linearized power flow model. Although the linear power flow model in [11] stands correct for most of the cases, it cannot rigorously guarantee the feasible operation of a generic power distribution grid in correspondence to any possible state. In this respect, the full AC power flow equations might be considered to properly model the grid constraints. However, this leads to the well-known non-convex optimal power flow (OPF) problem [13], [14]. OPF problems are usually computationally expensive; thus, they are often used for offline optimizations schemes such as for the planning of grid reinforcements (e.g., [15]). Several approaches have been proposed in the literature to address the non-convexity of power-flow equations [11], [16]–[20]. The first approach is based on its linearization, for example, in [11], [16], [17]. These schemes rely on the first (e.g. [11], [17]) or multiple (e.g. [16]) order Taylors series expansion of the power flow equations to express the nodal voltages, lines current, and losses as a function of the power injections. The second approach relies on the adoption of suitable relaxation of the power flow equations to obtain a convex formulation of the OPF [18]–[20]. Semidefinite relaxation, as second-order-cone-program (SOCP) in a bus injection model [19] and in a branch flow model [20] are the most adopted models. However, they apply to a subset of distribution networks. Furthermore, these methods ignore the presence of shunt elements, which is not a realistic assumption for MV distribution networks with branch

composed by long coaxial cables. To fix these shortcomings, in [18] it is proposed the so-called augmented relaxed (AR)-OPF, which accounts for the shunt elements and provides an exact solution of the OPF if specific conditions are met.

Given the above-listed issues, we propose an MPC scheme to achieve an accurate dispatch tracking of distribution grid while avoiding BESSs SOC saturation. The proposed scheme inherently restores adequate SOC levels for the subsequent day. It is achieved by a two-layer real-time MPC where the upper layer refines the SOC trajectory of the BESS every 5 minutes, based on updated forecasts of prosumers uncertainties for longer time horizons. Then, the lower layer MPC computes the BESS active and reactive power setpoints by considering the SOC trajectory computed by the upper layer as a constraint. The upper layer MPC is periodically fed with updated 5-minutes forecasts of the stochastic injections for a longer time horizon (up to the end of the day of operation). Regarding the forecasts, we adopted an integrated data-driven prediction of the prosumption relying on day-ahead predicted scenarios, updated global horizontal irradiance (GHI) forecasts from a commercial service, and the latest power measurements. The RT control scheme accounts for the grid constraints by means of the AR-OPF [18]. The proposed framework is experimentally validated on an actual 24-node medium voltage (MV) grid in Aigle, Switzerland, hosting uncontrollable 3.2 MWp distributed photovoltaic generation, 3.4 MVA hydro generations, and 2.8 MW base demand. A grid-connected 1.5 MVA/2.5 MWh BESS is the sole controllable resource in this setup. The grid is equipped with a state-of-the-art metering and communication infrastructure to determine the grid state at a high refresh rate (i.e., 50 estimations a second) by using distribution level phasor measurement units (PMUs).

The paper is organized as follows. Section II states the problem, Section III describes the day-ahead problem, Section IV introduces the real-time controller, Section V presents the experimental setup, Section VI discusses the experimental results and Section VII summarizes the outcomes and findings.

II. Problem statement

We consider a power distribution grid hosting heterogeneous controllable and uncontrollable DERs. The uncontrollable resources comprise stochastic renewable power generators and demand whereas the controllable resource is a grid-connected BESS. The grid is dispatched at its grid connection point (GCP) by controlling the BESS via a *real-time (RT) controller* according to a pre-determined *dispatch plan*. The dispatch plan is computed the day-ahead based on the forecasts of stochastic generation and demand, the status of the controllable resource (i.e., the BESS) and by taking into account the local grid constraints. The dispatch plan has a 5-minutes time resolution and is computed at 23:30 local time the day before operation.

The RT operation start at 00:00 local time. The objective of the RT controller is to achieve a fine tracking of the day-ahead dispatch plan while avoiding the saturation of the BESS SOC during the rest of the daily operation. Furthermore, at the end of the day, the framework has to restore a sufficient BESS SOC for dispatching the next day. Existing schemes in [9], [11] used a RT controller with an MPC look-ahead horizon of 5-minutes. However, this MPC is myopic to the uncertainties of the injections, eventually leading to BESS SOC saturation as schematically shown in Fig. 1. We want to avoid BESS SOC saturation by adding a farsighted MPC layer imposing an SOC budget. This feature is enabled by the proposed two-layered MPC framework where the upper layer (farsighted) takes care of the SOC saturation of the BESS, whereas the lower layer (myopic) aims to fine-track the dispatch plan.

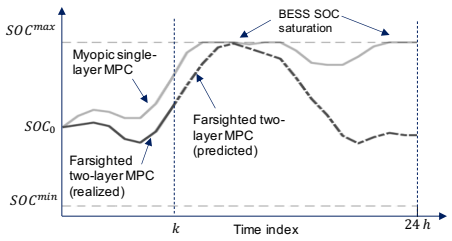

Fig. 1. Schematic representation of the SOC evolution of the BESS with myopic single-layer MPC and farsighted two-layer MPC.

- The *upper layer MPC* computes the BESS energy budget using the information on the intraday forecasts and current states of both grid and BESS. It runs every 5 minutes.
- The *lower layer MPC* optimizes the active and reactive power setpoints of the BESS while considering the energy budget restrictions from upper layer MPC and grid constraints. It runs every 30 seconds.

The day-ahead and real-time dataflow is shown in Fig. 2. Each stage is described in detail in the following sections.

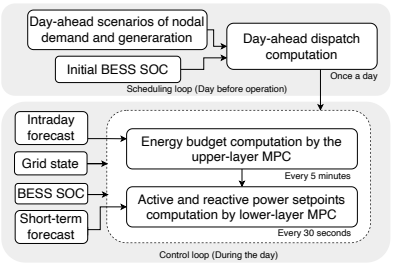

Fig. 2. Schematic dataflow of the proposed scheduling and control framework.

III. Day-ahead dispatch computation

The objective of the day-ahead scheduling is to compute the dispatch plan, namely the active power profile that the targeted distribution network should follow at its GCP at 5 minutes resolution during the next day operation. The dispatch plan is denoted by the sequence $P_k^{disp}, k = 0, 1, \ldots, N-1$ where index k is associated to 5-minute discrete intervals of the day of operation, and $N = 288$ is the number of time intervals in 24 hours. The dispatch plan accounts for the stochastic variations of the distributed renewable generations and demand by day-ahead scenarios produced according to forecasts.

A. Day-ahead load and renewable power generation forecast

The dispatch computation relies on power injection forecasts (for each node of the network) modeled by scenarios. We

develop a data-driven scheme to generate day-ahead scenarios of demand and renewable (in the form of PV and hydro) power generation. We assume that the PV generation is aggregated behind-the-meter with the local loads whereas the hydro power generation is from stand-alone distributed power plants.

1) Demand forecast: it uses nodal historical data-sets updated on a rolling horizon whenever new data is available. **Algorithm** 1 shows the key steps: the first one refers to the disaggregation of the true demand from the aggregated nodal injections (denoted by $\mathcal{P}_l$), followed by the clustering and multivariate Gaussian fitting of the true demand. These steps are described below.

Algorithm 1 Day-ahead demand forecasting

Require: Historical nodal power injections ($\mathcal{P}_l$), GHI ($\mathcal{G}$), air temperature (θ), node index $l \in \mathcal{L} = [1, \ldots, L]$

1: **procedure** DEMANDDAYAHEAD([1])
2: **for** l = 1:$|\mathcal{L}|$ **do**
3: **if** node l contains a PV plant **then**
4: $[\mathcal{P}_l^{load}$, PV-config] = Dissaggregation$(\mathcal{P}_l, \mathcal{G}, \theta)$
5: **else**
6: $\mathcal{P}_l^{load} = \mathcal{P}_l$
7: **end if**
8: $[\mathcal{P}_l^{C_1}, \ldots, \mathcal{P}_l^{C_{N_c}}]$ = Clustering($\mathcal{P}_l^{load}$, features)
9: **end for**
10: **for** $c = 1 : N_c$ **do**
11: $\Delta\mathcal{P}_l^{C_i} = \mathcal{P}_l^{C_i} - \texttt{mean}(\mathcal{P}_l^{C_i})$
12: $\Omega_l^{C_i} = \texttt{cov}(\Delta\mathcal{P}_l^{C_i})$ (multivariate Gaussian fitting)
13: $\Delta\tilde{\mathcal{P}}_l^{C_i} = \texttt{mvnrnd}(\Omega^{C_i}, N_{sc})$
14: $\tilde{\mathcal{P}}_l^{C_i} = \Delta\tilde{\mathcal{P}}_l^{C_i}$ + $\texttt{mean}(\mathcal{P}_l^{C_i})$
15: **end for**
16: **end procedure**

- **Disaggregation:** it separates the true demand from the behind-the-meter (BTM) PV generation. We use the unsupervised disaggregation (step 4 in **Algorithm** 1) process proposed in [21]. In brief, the method relies on the net nodal power injections ($\mathcal{P}_l$), GHI $\mathcal{G}$, and air temperature θ from the same area. It models the PV generation as a function of GHI (considering several tilt and azimuth of PV panels), enabling the identification of the patterns of the PV generation in the measured data set. As side result, it provides the disaggregated (or actual) demand that is used to develop the corresponding day-ahead forecast model.
- **Clustering:** is applied on the estimated demand profiles ($\mathcal{P}_l^{load}$) to group them into N_c clusters based on features (such as day-types in step 8, **Algorithm** 1). We use four clusters ($N_c = 4$): Mondays to Thursdays (C_1) are into one day type, Fridays (C_2), Saturdays (C_3) and Sundays (C_4) into other three separate day type clusters.
- **Multivariate-Gaussian-based scenario generation:** each day type cluster is fitted to a Multivariate-Gaussian model via the following steps: i) computation of the zero mean scenarios for the historical data set (step 11, **Algorithm** 1), ii) computation of the time cross-correlation matrix (step 12), iii) sampling of N_{sc} number of scenarios using the time-correlated multivariate Gaussian distribution model with a 95% confidence interval (step 13) and, finally, generate the demand scenarios by adding the cluster mean (step 14).

2) PV generation: is modeled starting from the day-ahead GHI forecasts provided by a commercial forecasting service, SoDa [22]. It provides forecasts for the present and the next day with a time resolution of 15-minutes and updated every 6 hours. The method uses gradient boosting as part of machine learning scheme and uses inputs such as historical data-sets of HelioClim-3 [23], McClear clear sky irradiance model [24], and Global Forecast Service (GFS) Numerical Weather Prediction (NWP).[2] It provides point predictions and 5% and 95% confidence intervals that are fundamental to generate scenarios when computing the dispatch plan. The 15-minutes forecasts are linearly interpolated to obtain estimates with 5-minutes time sampling. To convert the GHI forecasts to power generation, we use a physics-based model tool-chain [25] that takes air temperature (θ), tilt, and azimuth angles and nominal capacity of the PV plant. These parameters are obtained from the PV-config output from step 4, **Algorithm 1** as the true configurations of the PV plants are not known a-priory.

3) Hydro generation: In our forecast model, the hydropower plants are operated at a given power setpoint and do not have significant intra-day variation, so we model them as constant power injection sources.

A validation of the predicted scenarios using above forecasting methods are presented in Sec VI.

B. Day-ahead problem formulation

We use the dispatch computation algorithm from [26], a stochastic-based optimization problem accounting for the uncertainty of the nodal powers (modeled by day-ahead scenarios) and the grid constraints by co-dist-flow[3] [26]. The problem minimizes the dispatch error considering all the day-ahead scenarios and flexibility offered by the controllable resource. The dispatch plan is computed such that the power regulation made by the controllable resources (BESS in this case) does not violate the grid's and its constraints, and the power factor at the GCP remains within a pre-defined range. Since the main contribution of this work is on a real-time control scheme, we omit to include the dispatch formulation.

IV. REAL-TIME OPERATION

The real-time control objective is to track the day-ahead dispatch plan during the day of operation using a BESS. As stated earlier, the real-time control scheme comprises two layers operating at 5-minutes and 30 seconds time resolutions. The control problems of both layers are formulated as MPC and require forecasts of the nodal power injections. The upper layer MPC uses forecasts of the nodal power injections at 5-minutes time resolution, whereas the lower layer MPC uses forecasts at 30-seconds time resolution. We use data-driven schemes for *intra-day* and *short-term* forecasting for upper and lower MPCs respectively. They are described below.

[1]The functions `mean`, `cov` and `mvnrnd` are MATLAB functions to compute mean, correlation coefficients and for generating random scenarios based on a pre-computed standard deviation and number of samples, respectively.

[2]www.ncei.noaa.gov/products/weather-climate-models/global-forecast.

[3]The co-dist-flow is an iterative scheme where the dispatch plan is first optimized by neglecting the losses, then they are corrected by solving non-linear AC power flow which is accounted in the next iteration of the optimization. The reader can refer to [26] for more information.

A. Intra-day and short-time forecasting

A data-driven *intra-day forecasting* scheme has been developed to forecast nodal power injections during the day using the latest measurements of power ($\mathbf{p}_l^{meas}$) (provided by PMUs), updated GHI forecasts from SoDa [22] and day-ahead scenarios. The scheme in described in **Algorithm 2**. Intra-day forecasts $\hat{\mathbf{p}}_l^{load}$ is obtained as the weighted sum of the day-ahead scenarios of nodal injections ($\tilde{\mathcal{P}}_l$ from **Algorithm 1**). The weights are derived and updated every 5-minutes based on recent realization from the measurements. The weights are computed by finding the similarity (by norm-2) between the realization and day-ahead scenarios as in step 5, **Algorithm 2**. In step 7-12, updated GHI and air temperature forecasts are obtained from SoDA service, then used to compute PV generation ($\hat{\mathbf{p}}_l^{pv}$). Intra-day forecasts are updated every 5 minutes.

Algorithm 2 Intra-day forecasting

Require: Day-ahead load scenarios ($\tilde{\mathcal{P}}_l = [\mathbf{p}_{l,1}^{load}, \ldots, \mathbf{p}_{l,N_{sc}}^{load}]$), PV-config (from **Algorithm** 1)

1: **procedure** INTRADAYFORECAST
2: **for** l = 1:$|\mathcal{L}|$ **do**
3: Retrieve realizations ($\mathbf{p}_l^{meas}$) till the last 5-minutes slot.
4: $\mathbf{d} = [d_1, \ldots, d_i, \ldots, d_{N_{sc}}] = \|\tilde{\mathcal{P}}_l - \mathbf{p}_l^{meas})\|_2$
5: Weights $w_i = 1/d_i / \sum_i^{N_{sc}}(1/d_i)$
6: Intra-day load forecast $\hat{\mathbf{p}}_l^{load} = \sum w_i \mathbf{p}_{l,i}^{load}$
7: **if** node l contains a PV plant **then**
8: Get GHI, temperature ($\mathcal{G}, \theta$) forecasts from SoDa
9: $\hat{\mathbf{p}}_l^{pv}$ = PVmodel($\mathcal{G}, \theta$, PV-config)
10: **else**
11: $\hat{\mathbf{p}}_l^{pv} = 0$
12: **end if**
13: **end for**
14: **end procedure**

Short-term forecasts are obtained by linearly interpolating the latest intra-day forecasts with the time-resolution of 30 seconds and, then we use persistent predictor[4] to correct the forecasts of current timestep using the last observations. The short term forecasts are updated each 30 seconds.

B. Grid model

Both the MPC layers account for the grid constraints using AR-OPF [18] model, an exact convexification of the non-linear AC power flow equations. To introduce the AR-OPF nomenclature, we refer to generic two-port equivalent $\Pi-$model of the network branches shown Fig. 3. As anticipated before, we consider a radial grid configuration.

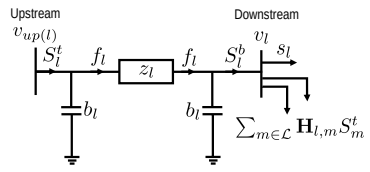

Fig. 3. Illustration of the adopted nomenclature with respect to the generic two-port Π model of a transmission line.

[4]More advanced forecaster will be investigated in future works.

Let index 0 refer to the slack bus. Buses other than the slack are denoted by $1, \ldots, L$ and are in the set $\mathcal{L}$. The upstream and downstream buses to bus l are denoted by symbol $up(l)$ and l respectively. The symbol $\mathbf{H}$ refers to adjacency matrix as defined in [18]. Let k be the time index in the set $\mathcal{K} = [1, \ldots, K]$. Let $S_{l,k}^t = P_{l,k}^t + iQ_{l,k}^t$ and $S_{l,k}^b = P_{l,k}^b + iQ_{l,k}^b$ be the complex power that is entering the line l from top and bottom respectively; and f_l be the square of the current in line l flowing through z_l (see Fig. 3). $z_l = r_l + ix_l$ and $2b_l$ be the longitudinal impedance and shunt capacitance of line l. z_l^* refer to complex conjugate of z_l. Let $v_{l,k}$ be the square of the voltage magnitude at bus l and v^{min} and v^{max} the squares of the minimum and maximum of nodal voltages. I_l^{max} is the square of maximum current limits of the line l. Let $s_{l,k} = p_{l,k} + iq_{l,k}$ be the power absorbed at bus l. Let $s_{l,k}^B = p_{l,k}^B + iq_{l,k}^B$ be the injections from BESS. The uncontrollable injections from demand, PV and hydro generation are modeled by their forecasts denoted as $\hat{p}_{l,k}^{load}$, $\hat{p}_{l,k}^{pv}$ and $\hat{p}_{l,k}^{hydro}$ respectively. The nodal active and reactive injections are $p_{l,k} = p_{l,k}^B + \hat{p}_{l,k}^{pv} + \hat{p}_{l,k}^{hydro} - \hat{p}_{l,k}^{load}$ and $q_{l,k} = -q_{l,k}^B - \hat{q}_{l,k}^{load} - \hat{q}_{l,k}^{hydro}$, respectively.

According to [18], the AR-OPF constraints are composed of the SOCP relaxation of power flow equation (referred as relaxed (R)-OPF). The R-OPF equations are

$$S_{l,k}^t = s_{l,k} + \sum_{m\in\mathcal{L}} \mathbf{H}_{l,m} S_{m,k}^t + z_l f_{l,k} - j(v_{up(l),k} + v_{l,k}) b_l, \tag{1a}$$

$$S_{l,k}^b = s_{l,k} + \sum_{m\in\mathcal{L}} \mathbf{H}_{l,m} S_{m,k}^t, \quad \forall l \in \mathcal{L}, \forall k \in \mathcal{K}, \tag{1b}$$

$$v_{l,k} = v_{up(l),k} - 2\Re\Big(z_l^* \Big(S_{l,k}^t + j v_{up(l),k} b_l\Big)\Big) + |z_l|^2 f_{l,k}, \quad \forall l \in \mathcal{L}, \forall k \in \mathcal{K}, \tag{1c}$$

$$f_{l,k} \geq \frac{|S_{l,k}^t + j v_{up(l),k} b_l|^2}{v_{up(l),k}}, \quad \forall l \in \mathcal{L}, \quad \forall k \in \mathcal{K}, \tag{1d}$$

For the exactness, the AR-OPF [18] introduces auxiliary variables to add security constraints on upper bounds of the nodal voltage and current magnitudes. It is done such that this upper bounds do not depend on original variable f rather an upper bound $\bar{f}$. Let symbols $\bar{f}, \hat{S}, \bar{S}$ are auxiliary variables for lines of the grid and $\bar{v}$ for the buses. The AR-OPF equations are defined as follows.

$$\hat{S}_{l,k}^t = s_{l,k} + \sum_{m\in\mathcal{L}} \mathbf{H}_{l,m} \hat{S}_{m,k}^t - j(\bar{v}_{up(l),k} + \bar{v}_{l,k}) b_l, \quad \forall l \in \mathcal{L}, \forall k \in \mathcal{K}, \tag{1e}$$

$$\hat{S}_{l,k}^b = s_{l,k} + \sum_{m\in\mathcal{L}} \mathbf{H}_{l,m} \hat{S}_{m,k}^t, \quad \forall l \in \mathcal{L}, \forall k \in \mathcal{K}, \tag{1f}$$

$$\bar{S}_{l,k}^t = s_{l,k} + \sum_{m\in\mathcal{L}} \mathbf{H}_{l,m} \bar{S}_{m,k}^t + z_l f_{l,k} - j(v_{up(l),k} + v_{l,k}) b_l, \quad \forall l \in \mathcal{L}, \forall k \in \mathcal{K}, \tag{1g}$$

$$\bar{S}_{l,k}^b = s_{l,k} + \sum_{m\in\mathcal{L}} \mathbf{H}_{l,m} \bar{S}_{m,k}^t, \quad \forall l \in \mathcal{L}, \forall k \in \mathcal{K}, \tag{1h}$$

$$\bar{v}_{l,k} = \bar{v}_{up(l),k} - 2\Re\Big(z_l^* (\hat{S}_{l,k}^t + j\bar{v}_{up(l),k} b_l)\Big), \quad \forall l \in \mathcal{L}, \forall k \in \mathcal{K}, \tag{1i}$$

$$\bar{f}_{l,k} v_{l,k} \geq |\max\{|\hat{Q}_{l,k}^b - j\bar{v}_{l,k} b_l|, |\bar{Q}_{l,k}^b - j v_{l,k} b_l|\}|^2 + |\max\{|\hat{P}_{l,k}^b|, |\bar{P}_{l,k}^b|\}|^2, \quad \forall l \in \mathcal{L}, \forall k \in \mathcal{K}, \tag{1j}$$

$$\bar{f}_{l,k} v_{up(l),k} \geq |\max\{|\hat{Q}_{l,k}^t + j\bar{v}_{up(l),k} b_l|, |\bar{Q}_{l,k}^t + j v_{up(l),k} b_l|\}|^2 + |\max\{|\hat{P}_{l,k}^t|, |\bar{P}_{l,k}^t|\}|^2, \quad \forall l \in \mathcal{L}, \forall k \in \mathcal{K}, \tag{1k}$$

$$I_l^{max} v_{up(l),k} \geq |\max\{|\hat{P}_{l,k}^t|, |\bar{P}_{l,k}^t|\}|^2 + |\max\{|\hat{Q}_{l,k}^t|, |\bar{Q}_{l,k}^t|\}|^2, \quad \forall l \in \mathcal{L}, \forall k \in \mathcal{K}, \tag{1l}$$

$$I_l^{max} v_{l,k} \geq |\max\{|\hat{P}_{l,k}^b|, |\bar{P}_{l,k}^b|\}|^2 + |\max\{|\hat{Q}_{l,k}^b|, |\bar{Q}_{l,k}^b|\}|^2, \quad \forall l \in \mathcal{L}, \forall k \in \mathcal{K}, \tag{1m}$$

$$v^{min} \leq v_{l,k}, \ \ \bar{v}_{l,k} \leq v^{max}, \quad \forall l \in \mathcal{L}, \forall k \in \mathcal{K}, \tag{1n}$$

$$\bar{P}_{l,k}^t \leq P_l^{max}, \quad \bar{Q}_{l,k}^t \leq Q_l^{max}, \quad \forall l \in \mathcal{L}, \forall k \in \mathcal{K}, \tag{1o}$$

Eq. 1e-(1f) express the lower bound on branch power flows at the sending and receiving ends of the line l, whereas the eq. (1g) and (1h) express the upper bound for power flows. Eq (1i) expresses the upper bound on the nodal voltages. These variables are then used in upper and lower bounds on the square of longitudinal current in eq. (1j) and (1k). Eq. (1l)-(1m) and eq. (1n) impose limits on the amapacities and nodal voltage respectively. Eq. (1o) expresses upper bound on the active and reactive power flows in line l where P_l^{max}/Q_l^{max} are bounds on active/reactive power flows in line l.

C. Model Predictive Control (MPC) of BESS

1) BESS model: the BESS is controlled by an MPC to provide active and reactive power regulations to the grid while respecting the capability of the BESS power converter. Let P_l^{bess} and E_l^{bess} be the power and energy capacities of BESS connected at bus l. In theory, the converter capability is represented by a circle ($(p_{l,k}^B)^2 + (q_{l,k}^B)^2 \leqslant {P_l^{bess}}^2$), but it is not true in practice as the power capability of the converter depends on both the AC and DC voltages of the converter. An example of capability curves with different combination of the AC and DC voltage are shown in Fig. 4a, and they can be represented by piece-wise-linear functions as follows.

$$\phi(v_t^{dc}, v_t^{ac}, p_l^B, q_l^B, P_l^{bess}) \leq 0. \tag{2a}$$

Here, v^{dc} is the DC bus voltage and v_t^{ac} is the magnitude of the direct sequence voltage on the AC side of the converter. They can be obtained from measurements.

We model the BESS losses by adding an equivalent resistance in the power flow equations as proposed in [26]. The approach integrates the equivalent resistance into the grid's admittance matrix by adding a extra line (l') for each BESS. It allows retaining the convexity of the AR-OPF problem without the need of any auxiliary variables. Fig. 4 shows the equivalent resistance with an ideal voltage source and series resistance (R_l^{bess}). Thanks to this simplification (i.e., adding equivalent

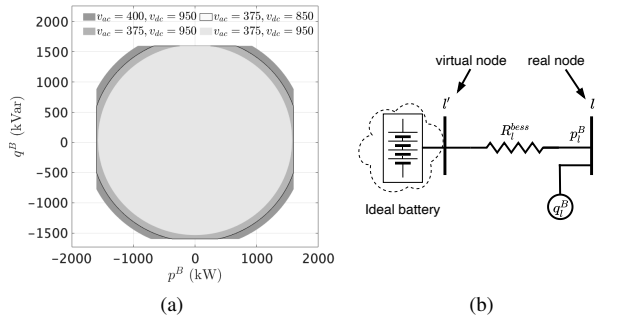

(a) (b)

Fig. 4. (a) BESS converter capability function ϕ in eq.2a with AC and DC voltages. (b) Equivalent circuit diagram of BESS.

resistance into the grid's admittance matrix) the BESS state-of-energy (SOE) evolution with sampling time T_s is now expressed simply by

$$SOE_{l,k+1} = SOE_{l,k} + T_s p_{l,k}^B, \qquad \forall l \in \mathcal{L}, \forall k \in \mathcal{K}. \tag{2b}$$

We constrain the SOE by safety margin of 0.1 per unit of the extremes saturation/depletion of the battery. It is

$$0.1E_l^{bess} \leq SOE_{l,k} \leq 0.9E_l^{bess}, \qquad \forall l \in \mathcal{L}, \forall k \in \mathcal{K}, \tag{2c}$$

Also, to account for the degradation of the BESS caused by its operation, we include the following constraint that limits the active power by a pre-defined threshold:

$$\frac{T_s}{2 \times 3600} \left| p_{l,k}^B \right| \leq N_e E_l^{bess}, \qquad \forall l \in \mathcal{L}, \forall k \in \mathcal{K} \tag{2d}$$

where N_e is rated number of cycles for the battery.

2) Model Predictive Control (MPC) Problem: as stated earlier, the real-time control scheme comprises two layers, both formulated as MPC but with different horizon lengths. The upper layer considers intra-day prosumption forecast along the whole day via subsequent shrinking horizon and computes successive BESS SOC trajectories. The lower layer considers forecast of 5-minutes interval with a shrinking horizon and computes power setpoints for the BESS while accounting for the SOC trajectory (provided by the upper layer) as hard constraint. This two-layered structure enables full visibility of the uncertainties during the real-time operation, therefore ensuring the BESS SOC to not saturate. Fig. 5 explains the sequence of operations during real-time operation per time step. The time intervals are divided into 5-minutes and 30-seconds slots corresponding to the sampling of upper and lower level MPCs.

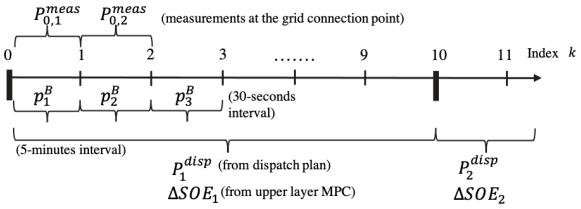

Fig. 5. Sequence of decisions computed during real-time operations.

- The dispatch setpoint to track P_k^{disp} is retrieved from the dispatch plan profile with indices $k = 0, 1, \ldots, N-1$ where $N = 288$ for 24 hours in a day. Intra-day forecasts $\hat{p}_{l,k}^{load}, \hat{q}_{l,k}^{load}, \hat{p}_{l,k}^{pv}, \hat{p}_{l,k}^{hydro}$, are updated.
- The upper layer MPC computes BESS energy budget $\Delta SOE_k, \ k = 0, 1, \ldots, N-1$ every 5-minutes based on updated intra-day forecasts and current BESS SOE.
- The dispatch setpoint to track by the lower MPC is denoted by $\bar{P}_k^{disp} = P_{\lfloor \frac{k}{10} \rfloor}^{disp}$, where $\lfloor . \rfloor$ refers to the floor funtion. The first and the last 30-seconds index in current 5-minutes interval are denoted by $\underline{k}$ and $\bar{k}$ respectively, i.e., $\underline{k} = \lfloor \frac{k}{10} \rfloor \times 10$ and $\bar{k} = \underline{k} + 10 - 1$. The power measurements at the GCP denoted by $P_{0,k}^{meas}$ is obtained. Using $\bar{P}_k^{disp}, P_{0,k}^{meas}$ and ΔSOE_k, it computes BESS setpoints p_k^B at time resolution of 30 seconds with indices $k = 0, 1, \ldots, K-1 \in \mathcal{K}$ with $K = 2880$ for a 24 hours operation day.

a) Upper layer MPC: the objective is to minimize the tracking error between the dispatch plan P^{disp} and power at the GCP P_0^t. Note that P_0^t is a dependent variable related to the uncontrollable power injections, the controllable BESS injections and the grid losses derived from AR-OPF (Eq.(1)). The decisions variables are the BESS active and reactive powers to compensate for the uncertainties in the nodal injections,

the latter modeled by intraday point forecasts. The objective function to minimize is the weighted[5] sum of the tracking error for the whole day and grid losses[6]:

$$\widehat{p}_l^B = \underset{\forall S,v,s^B}{\arg\min}\ w_p \sum_{j=k}^{N} \|P_j^{disp} - P_{0,j}^t\|_2 + w_l \sum_{j=k}^{N} \sum_{l\in\mathcal{L}} r_l f_{lj} \quad (3a)$$

$$\text{subject to} \quad (1), (2) \quad (3b)$$

A bound on the final SOE such that it is restored to comfortable SOC by the day's operation is also added.

$$0.45E_l^{bess} \leq SOE_{l,N} \leq 0.55E_l^{bess}. \quad (3c)$$

The state of energy budget ΔSOE_l is computed using the first element of the BESS setpoint vector from upper-layer MPC:

$$\Delta\widehat{SOE}_l = \widehat{p}_{l,1}^B \times \frac{300}{3600}. \quad (3d)$$

b) Lower layer MPC: The problem is formulated as an MPC and its objective is to minimize the energy error incurred over a 5 minutes horizon length with power set-points actuated each 30 sec. The dispatch energy error at time k comprises of *(i)* uncovered energy error from time index $\underline{k}$ to $k-1$, $\hat{\epsilon}_k = \sum_{j=\underline{k}}^{k-1}(\bar{P}_j^{disp} - P_{0,j}^{meas})$ and *(ii)* the predicted error from k to $\bar{k}$ given as $\epsilon_k = \sum_{j=k}^{\bar{k}}(\bar{P}_j^{disp} - P_{0,j}^t)$. The MPC objective is a multi-objective function comprised of the dispatch energy error incurred at the GCP (from current timestep to end of the 5-min period) and the grid losses:

$$\underset{\forall S,v,s^B}{\text{minimize}}\ w_e(\epsilon_k + \hat{\epsilon}_k) + w_l \sum_{k\in\mathcal{K}} \sum_{l\in\mathcal{L}} r_l f_{l,k} \quad (4a)$$

$$\text{subject to} \quad (1), (2). \quad (4b)$$

Additionally, the energy budget from the upper layer MPC are added as constraint imposed on the BESS SOE as:

$$SOE_{l,\bar{k}} \geq SOE_{l,\underline{k}} + \Delta\widehat{SOE}_l \quad \text{if} \quad \Delta\widehat{SOE}_l \geq 0, \quad (4c)$$

$$SOE_{l,\bar{k}} \leq SOE_{l,\underline{k}} + \Delta\widehat{SOE}_l \quad \text{if} \quad \Delta\widehat{SOE}_l \leq 0. \quad (4d)$$

The constraints in (4c) sets a threshold SOC to be attained by the end of current 5-minutes duration. It ensures that the BESS is used judiciously by the lower MPC to avoid its saturation and therefore restoring to comfortable SOC value by the end of the daily operation. Thanks to the convex reformulation of the AC power flow equations using AR-OPF, the control problems in (3) and (4) are convex and can be solved by standard solvers.

V. Experimental Setup

A. Medium voltage distribution grid in Aigle, Switzerland

We validate the proposed control scheme on a real MV grid situated in Aigle, Switzerland, a mixed rural/urban system operated by Romande Energie,[7] one of the main Swiss DSOs. We consider a radial feeder composed by 24 nodes. The topology and locations of various connected resources are shown in Fig. 6a-6b. It is a three-phase 21 kV/20 MVA balanced (seen in the observations) system. The grid accommodates peak power consumption (at the feeder) of 4.3 MWp and 2.9 MWp during the winter and summer, respectively. It hosts aggregated PV generation capacity of 3.2 MWp including a single plant of 1.8 MWp. The grid also hosts distributed hydropower generation of 3.4 MVA allocated in 4 plants. The placement of these generations are shown in Fig. 6a. The grid is connected with a 1.5 MW/2.5 MWh BESS at node 11. Figure 6c shows exterior and interior of the BESS. The cells are Lithium-Nickel-Manganese-Cobalt-Oxide (Li-NMCo) based and are rated for 4000 equivalent full cycles. It consists in 30 racks in parallel with 11 modules per rack in series (each module composed by 1p22s cell pack) connected to a four-quadrant power converter. The whole setup is installed in a temperature controlled container as shown in Fig. 6c.

B. Metering and IT infrastructure

1) Phasor measurement units: The real-time MPC algorithm relies on the grid-awareness provided by a cluster of distributed metering units providing up-to-date relevant measurements such that they can be accounted as initial conditions in the MPC problem while optimizing the power set-points from the controllable resources and ensuring safe and secure operation of the grid. In this respect, the MV distribution grid is equipped with the state-of-the-art monitoring solution SynchroGuard[8] that provides real-time situational awareness of the grid. The setup contains 17 PMUs distributed across the grid, the locations are shown in Fig. 6a. The PMUs provide synchronised and time-tagged phasors which are sent to a central server using a telecom network (fiber optic or 4G). Fig 7a shows an example of the PMU and its components at a substation. A real-time state estimator (RTSE) accurately estimates nodal voltage and nodal/branch current and powers of the whole grid every 20 ms using only the PMU data. The performance analysis of the RTSE is detailed in [27].

It is worth noting that the metering system is also a source of historical data that is used to obtain day-ahead scenarios, intra and short-term forecasts of the uncontrollable injections.

2) GHI and temperature measurement box: For modelling of the PV generation, we use historical data of GHI and air temperature from the same region where PV plants are located. So, we installed GHI and temperature sensing boxes (Meteobox) to measure the GHI, air- and PV-panel- temperatures. These meteoboxes are installed at three locations in the grid. They provide in real-time measurements with sampling of 500 ms (including communication latency). Fig 7b shows the installed meteobox at the site; each one consists of a pyranometer to sense the GHI, two temperature sensors, and a power supply. It also contains a modem which is used to stream the measured data using public 4G network to our data server. The meteobox code is implemented in NI compact RIO.

3) Communication infrastructure, centralized server and data-logging: Fig. 8 shows the schematic of communication and server infrastructure to enable the day-ahead and real-time control operations. A centralised server hosts four different virtual machines (VMs) to implement real-time state estimation (State-estimator), data logging (Database), day-ahead dispatch and real-time control computations (Controller) and

[5]The weights w_p, w_l and w_e may be derived from energy imbalance price in day-ahead electricity market.

[6]Grid losses are included to satisfy exactness conditions of the AR-OPF formulation as in [18]

[7]https://www.romande-energie.ch/.

[8]https://zaphiro.ch/technology/.

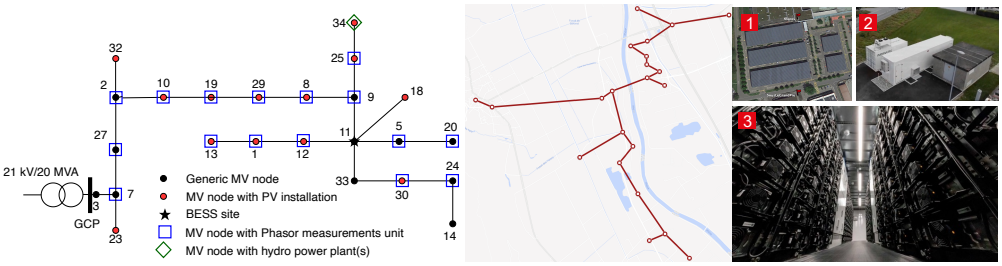

Fig. 6. (a) Topology with locations of the PMUs, PV plants, hydro-power plants, (b) Location of the substations and lines on the map, and (c) BESS and PV infrastructure: (1) Satellite view of the centralized PV plant of capacity 1.8 MWp, (2) battery container and (3) interior of the battery.

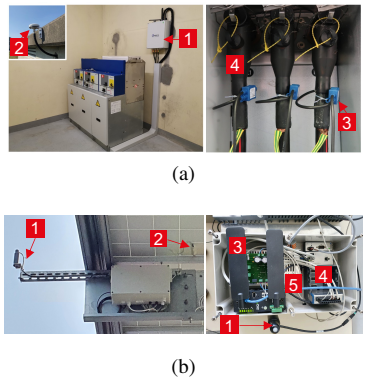

Fig. 7. (a) PMU installation at a monitored substation, 1) Zaphiro PMU box 2) GPS antenna, (3) current sensor (4) cables and (b) GHI and temperature measurement box (Meteobox) at a PV plant: 1) pyranometer, (2) temperature sensor (3) antenna (4) power supply (5) NI Compact RIO.

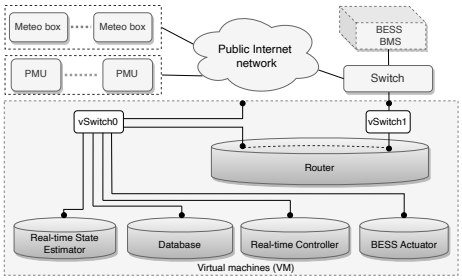

Fig. 8. IT communication infrastructure for the experimental setup (vSwitch refer to virtual switches).

BESS setpoint actuator (Actuator). To facilitate communication among VMs, BMS, PMUs and Meteoboxes, we equip it with dedicated IPv4 communication network as shown in Fig. 8. The communication network links all the monitoring units (PMUs and Meteoboxes), controllable resources (BESS' BMS and its converter). The PMUs and the Meteoboxes use public telecom network (fiber optic or 4G), whereas BESS use Ethernet cables. The Database VM gathers all the time series generated by the monitoring units. The VM state estimator does RTSE. The codes for forecasting (day-ahead to short-term), dispatch computation and real-time operation are running on Controller VM. The BESS Actuator VM receives the power set-points from the real-time controller, verifies its feasibility and implements it.

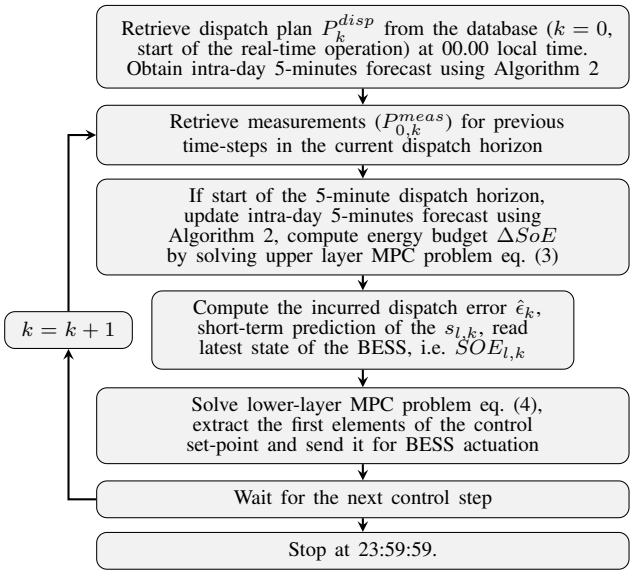

Fig. 9. Flow-chart showing real-time operation during 24 hours.

C. Dataflow

Fig. 9 shows the sequence of the operations and communication flow at the day-ahead and real-time stages. In the day-ahead scheduler (first step), the dispatch plan is computed and stored in the database. The input to the day-ahead stage are the forecast scenarios of the load and generation of different nodes (Sec. III-A) and the estimated state of the BESS. The day-ahead stage is run once a day at 23.30 local time. The real-time stage (second step onward) shows the steps during real-time operations. In the beginning of 5-minutes time interval, the energy budget is computed by the upper layer MPC based on latest intraday forecasts and current SOC. Then, the lower layer MPC loops every 30 seconds to compute BESS active and reactive setpoints based on short-term forecasts and BESS SOC. This cycle is repeated till 23:59:30 local time.

VI. Experimental Results

A. Experimental validation

This section presents the experimental results obtained by dispatching the MV grid described in Sec. V. First, we show results for two typical days representing different characteristics in terms of power injection patterns. On the first day,

it imports net power into the grid, whereas on the second day, it exports net power during the middle of the day, thanks to generations from hydro and PV plants. Then, we show control performance for a week-long experiment. The control performance of the proposed two-layer MPC scheme is compared against other two cases: (i) **Without control**, where no compensation from BESS is performed, and (ii) a **Single-layer MPC**, solving lower-layer MPC problem (eq. 4) but without SOE budget from upper layer MPC. Since the experiments were performed with the two-layer MPC, and the same experimental conditions can not be reproduced, we perform numerical simulations with single-layer MPC with same conditions as the day of operation for this comparison.

1) Day 1: corresponds to a clear-sky and weekday, where the demand is relatively higher than the net generations. The main source of uncertainty is the demand. The experimental results are described below.

a) Day-ahead operation: starts at 23.30 local time the day before. It computes the dispatch plan based on predicted scenarios. We show the day-ahead scenarios (lineplots in different colors) at the GCP[9] in Fig. 10a. The computed dispatch plan is shown in Fig. 10b along with the power at the GCP with contribution from the BESS. As it can be observed, the dispatch plan still have some uncovered error because of the insufficient size of the BESS. The SOC plot shown in the Fig. 10c shows that BESS is reaching its saturation limits with many scenarios. The initial SOC is 50 % which is also the SOC of the battery before the start of the real-time operation.

b) Real-time operation: starts at 00.00 hrs. Fig 11a shows the dispatch plan (in gray area), power at the GCP for different control schemes. Fig. 11b shows the SOC evolution with different control schemes. Fig 11c shows the plot of tracking error cumulative distribution function (CDF) as result of different real-time controls. As it can be observed, the single-layer MPC lets the BESS saturate at around 8:00 hrs and it could not be used for the whole day; hence failing the dispatch. In contrast, the two-layer MPC ensures the BESS to never saturate, thanks to the energy budget constraints computed by the upper layer MPC. Also, by looking at the CDF plot of the tracking error in Fig. 11c, it is clear that two-layer MPC, on the one hand, achieves better tracking of the dispatch plan with a lower probability of high tracking error. On the other hand, it keeps the BESS SOC within a flexible range. Table I reports the maximum-absolute-error (MAE), net absolute-energy-error (AEE), root-mean-square-error (RMSE) of the dispatch error using different controls concluding that the control based on two-layer MPC performs the best. The two-layer MPC outperforms the single-layer MPC in RMSE by 40%, MAE by 67% and AEE by 35% respectively.

2) Day 2: corresponds to a day with higher variation in the power injection due to higher uncertainty with next export due to high PV and hydro generations. The results are below.

a) Day-ahead operation: Fig 12a shows the day ahead scenarios for day 2. As it can be seen, this day exhibit more variations in power injections resulting in higher uncertainty in the day-ahead scenarios of the GCP. Also, during the middle of the day, the net power at the GCP is negative (producing) as hydro power plants at node 34 are generating. Fig 12b shows the computed dispatch plan and compressed scenarios of active powers at the GCP, thanks to the compensations from BESS. However, again the BESS capacity is not enough to cover the uncertainty of all the day-ahead scenarios resulting in spread of the optimized power at the GCP even with contribution of the BESS. It is also evident from the BESS SOC plot in Fig. 12c that the it saturates for several day-ahead scenarios.

[9]Due to space constraints, the day-ahead scenarios for the all the nodes of Aigle grid are not shown. The day ahead scenarios at the GCP is a by-product of the day-ahead scenarios at all the nodes accounting for the grid losses.

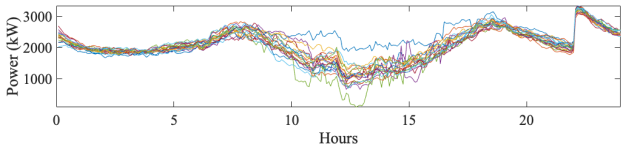

(a) Day-ahead aggregated prosumption scenarios ($\widehat{P}_0$) at the GCP.

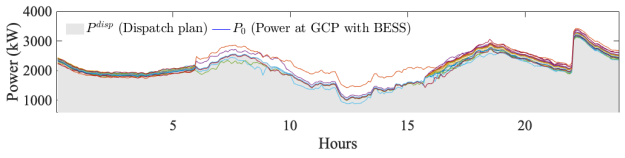

(b) Computed dispatch plan (in gray area) and scenarios at the GCP.

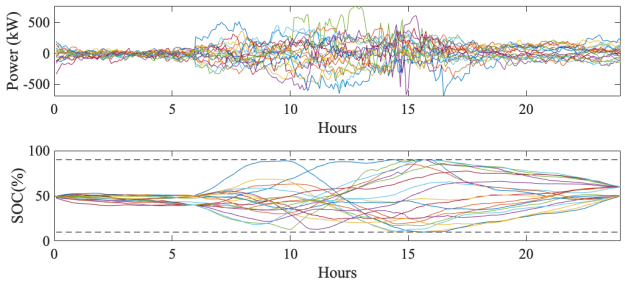

(c) Battery active power injection p^B (top) and SOC (bottom) for different day-ahead scenarios.

Fig. 10. (a-c) Dispatch plan computation for day 1 (01-Mar.-2022). Each line-plot in different color represents a different day-ahead scenario.

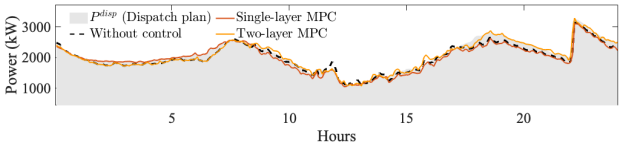

(a) GCP power tracking the dispatch plan with different control schemes.

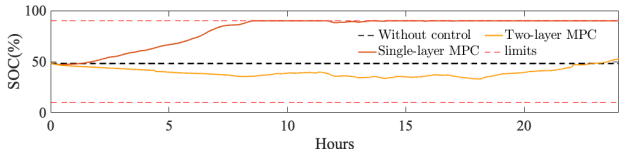

(b) SOC of the BESS with different control schemes.

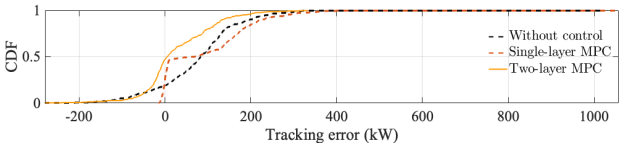

(c) CDF plot of the dispatch tracking error with different control schemes.

Fig. 11. (a-c) Real-time operation for day 1 (01-Mar.-2022).

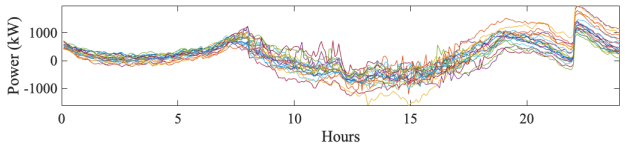

(a) Day-ahead aggregated prosumption scenarios ($\widehat{P}_0$) at the GCP.

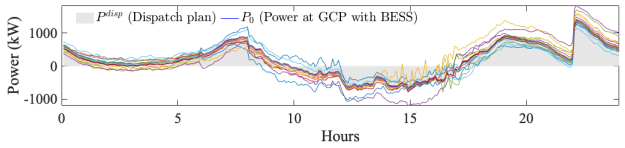

(b) Computed dispatch plan (in gray) and scenarios at GCP.

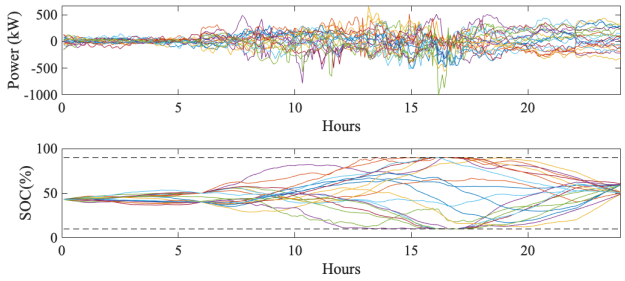

(c) Battery active power injection p^B (top) and SOC (bottom) for different day-ahead scenarios.

Fig. 12. (a-c) Dispatch plan computation for day 2 (22-Mar.-2022). Each line-plot in different color represents a different day-ahead scenario.

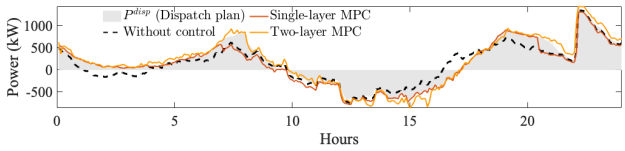

(a) GCP power tracking the dispatch plan with different control schemes.

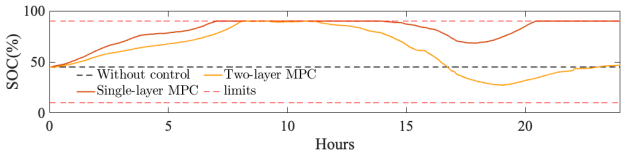

(b) SOC of the BESS with different control schemes.

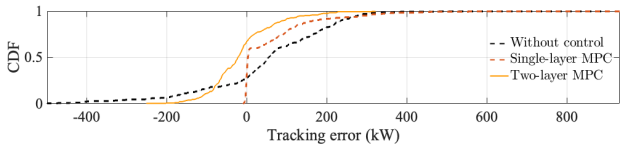

(c) CDF plot of the dispatch tracking error with different control schemes.

Fig. 13. (a-c) Real-time operation for day 2 (22-Mar.-2022).

b) Real-time operation: Fig 13a shows the tracked dispatch plan using different control schemes. Again, we show the BESS SOC, and the CDF of the dispatch tracking errors in Fig. 13b and 13c respectively. As observed, the two-layer MPC achieves fine-tracking of the dispatch plan compared to the other two cases. Moreover, the two-layer MPC restores the BESS SOC to 47% at the end of the day's operation, whereas the single-layer MPC lets the BESS to saturate to the upper limit (90%) from 7.00 hrs to 14.00 hrs and again from 20.00 hrs to 24.00 hrs; hence failing the dispatch during this period. The CDF plot in Fig. 13c shows that two-layer MPC achieves lower tracking error with high probability. The

TABLE I
TRACKING ERROR STATISTICS WITH DIFFERENT CONTROL SCHEMES.

MPC	Day 1			Day 2		
	RMSE (kW)	AEE (kWh)	MAE (kW)	RMSE (kW)	AEE (kWh)	MAE (kW)
None	137	2.5e3	1e3	176	3.2e3	896
Single-layer	148	2.3e3	1e3	124	1.5e3	932
Two-layer	89	1.5e3	332	85	1.5e3	322

metrics reported in Table I show that the two-layer MPC scores better on RMSE and MAE by 31% and 65% respectively than the single-layer MPC, however similar AEE.

3) Week-long experiment: To demonstrate the effectiveness of the dispatching scheme, we run the control of the BESS for a whole week. Fig 14a shows the dispatch plan, measured GCP power with and without two-layer MPC scheme. In Fig. 14b, we show the SOC evolution during the week. It can be observed that the power at the GCP follows the dispatch plan and the keeps the BESS SOC within comfortable SOC so that dispatching is continued the next day.

B. Further analysis

1) Validation of the grid model: We compare the modelled grid quantities by AR-OPF with the measurements to validate that the grid constraints are accounted correctly with minimum error. Fig. 15 shows comparison in form of CDFs for the difference between (modelled vs state estimated) the voltage, current and losses. The CDF plots on voltages and currents correspond to a particular bus/line. It can be seen that the modeled voltages and currents achieve high accuracy. The error on the voltage and current modelling are less than 0.01 pu and on the losses less than 0.2 kW for 99 % of the time. This comparison validates that the OPF model used to model the grid constraints in real-time MPC are realistic.

TABLE II
COMPUTATION TIME.

Control layers	Min (sec.)	Mean (sec.)	Max(sec.)
Upper-layer MPC	4	9.9	19
Lower-layer MPC	0.15	0.2	0.4

2) Computational performance: Table II lists the minimum, mean and maximum computation time to solve upper and lower layer MPCs. As it can be seen, the computation time is within 30 seconds, the time-deadline of real-time actuation.

VII. CONCLUSIONS

This work provided a solution to tackle the issue of BESS SOC saturation in dispatching ADNs, where a day-ahead dispatch plan is tracked with the help of a controllable BESS during the day's operation. The solution relies on a two-layer real-time MPC scheme, where a slow and farsighted MPC imposed an energy budget, every 5-minutes based on latest whole day forecasts, on the real-time fast MPC running every 30-seconds. The two-layer scheme ensures that the BESS SOC is not saturated during the day and restored to a comfortable SOC for the next day's dispatch operation. This is useful for reliable and continuous dispatching of ADNs by BESS. The MPCs are fed by data-driven forecasts of the demand and generations. The real-time control scheme accounted for the grid

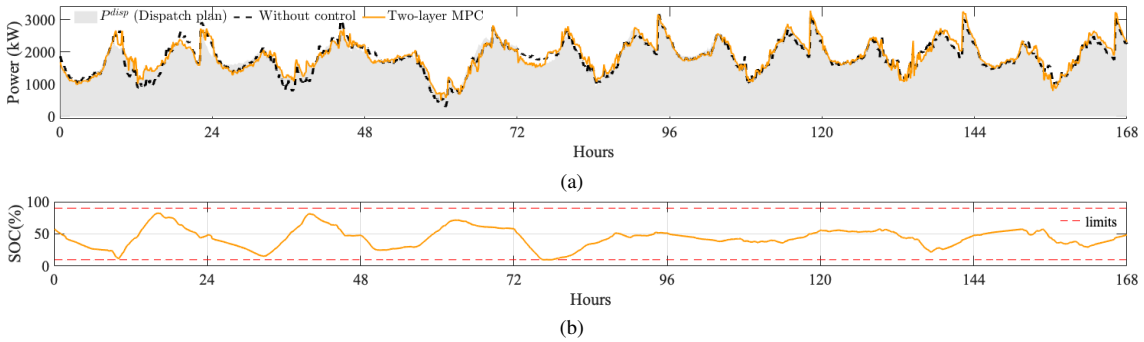

Fig. 14. Dispatch tracking over a week (25-Feb.-2022, Friday to 03-Mar.-2022, Thursday): (a) Power at the GCP and dispatch plan, (b) SOC evolution.

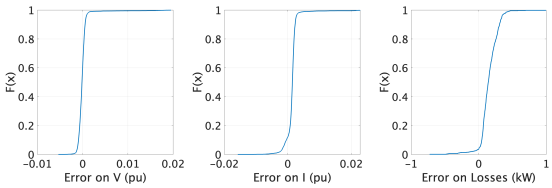

Fig. 15. Validation of OPF model for real-time operation with PMU measurements: (a-c) shows CDF of the incurred error on the modeling of voltage (in pu), current (in pu) and total grid losses (in kW).

constraints using a convex AC-OPF model. The optimization problem is formulated as convex, achieving optimality and enhanced level tractability and efficient to solve.

The control framework is validated on a real MV grid located in Aigle Switzerland hosting 3.2 MWp of photovoltaic generation, 3.4 MVA hydro generation and 2.8 MW of base demand. The MV grid is connected with 1.5 MVA/2.5 MWh BESS that is controlled by the real-time controller, and monitored by 17 PMUs. The experimental results performed over a week (including clear-sky, cloudy, weekday and weekend days) show that the proposed two-layer MPC scheme always keeps the BESS SOC within flexible region as well as achieves better tracking compared to myopic single-layer MPC scheme. The proposed two-layer MPC scheme reduces the absolute energy tracking error, MAE and RMSE by half compared to the myopic single-layer MPC scheme. We also validated the grid model by comparing the modeled vs estimated states, concluding the error below 0.01 per unit in the nodal voltages/lines currents and below 0.2 kW in the grid losses.

References

[1] A. Amin, "Renewable energy prospects for the european union," *IRENA Tech. Rep*, 2018.

[2] Y. Sun, S. V. Wachche, A. Mills, and O. Ma, "2018 renewable energy grid integration data book," NREL, CO (USA), Tech. Rep., 2020.

[3] AEMO, "Review of the black system south australia report – system event of 28 september 2016," Tech. Rep., 2017.

[4] CAISO, "Frequency response phase 2," Tech. Rep., 2016.

[5] J. Morren and S. De Haan, "Impact of distributed generation units with power electronic converters on distribution network protection," 2008.

[6] E. Coster and D. Van Houwelingen, "Integration of dg in mv-grids: Challenges encountered by the grid operator," in *2009 CIGRE/IEEE PES Joint Symposium*. IEEE, 2009, pp. 1–9.

[7] A. Nottrott, J. Kleissl, and B. Washom, "Energy dispatch schedule optimization and cost benefit analysis for grid-connected, photovoltaic-battery storage systems," *Renewable Energy*, vol. 55, pp. 230–240, 2013.

[8] E. Reihani, S. Sepasi, L. R. Roose, and M. Matsuura, "Energy management at the distribution grid using a battery energy storage system (bess)," *IJEPES*, vol. 77, pp. 337–344, 2016.

[9] F. Sossan, E. Namor, R. Cherkaoui, and M. Paolone, "Achieving the dispatchability of distribution feeders through prosumers data driven forecasting and model predictive control of electrochemical storage," *IEEE Trans. on Sust. Energy*, vol. 7, no. 4, pp. 1762–1777, 2016.

[10] M. Bozorg *et al.*, "Influencing the bulk power system reserve by dispatching power distribution networks using local energy storage," *Electric Power System Research*, vol. 163, pp. 270–279, 2018.

[11] R. Gupta, F. Sossan, and M. Paolone, "Grid-aware distributed model predictive control of heterogeneous resources in a distribution network: Theory and experimental validation," *IEEE Transactions on Energy Conversion*, vol. 36, no. 2, pp. 1392–1402, 2020.

[12] T. G. Paul *et al.*, "A quadratic programming based optimal power and battery dispatch for grid-connected microgrid," *IEEE Trans. Ind. App.*, vol. 54, no. 2, pp. 1793–1805, 2017.

[13] H. W. Dommel and W. F. Tinney, "Optimal power flow solutions," *IEEE Trans. Power App. Syst.*, no. 10, pp. 1866–1876, 1968.

[14] M. Huneault and F. D. Galiana, "A survey of the optimal power flow literature," *IEEE Trans. Power Syst.*, vol. 6, no. 2, pp. 762–770, 1991.

[15] S. P. Torres and C. A. Castro, "Expansion planning for smart transmission grids using ac model and shunt compensation," *IET Generation, Transmission & Distribution*, vol. 8, no. 5, pp. 966–975, 2014.

[16] R. A. Jabr, "High-order approximate power flow solutions and circular arithmetic applications," *IEEE Trans. Power Syst.*, vol. 34, no. 6, pp. 5053–5062, 2019.

[17] A. Bernstein *et al.*, "Load flow in multiphase distribution networks: Existence, uniqueness, non-singularity and linear models," *IEEE Trans. Power Syst.*, vol. 33, no. 6, pp. 5832–5843, 2018.

[18] M. Nick *et al.*, "An exact convex formulation of the optimal power flow in radial distribution networks including transverse components," *IEEE Trans. Autom. Control*, vol. 63, no. 3, pp. 682–697, 2017.

[19] R. A. Jabr, "Radial distribution load flow using conic programming," *IEEE Trans. Power Syst.*, vol. 21, no. 3, pp. 1458–1459, 2006.

[20] L. Gan, N. Li, U. Topcu, and S. H. Low, "Exact convex relaxation of optimal power flow in radial networks," *IEEE Transactions on Automatic Control*, vol. 60, no. 1, pp. 72–87, 2014.

[21] F. Sossan *et al.*, "Unsupervised disaggregation of photovoltaic production from composite power flow measurements of heterogeneous prosumers," *IEEE Trans. Ind. Inf.*, vol. 14, no. 9, pp. 3904–3913, 2018.

[22] "Solar radiation data (soda)." [Online]. Available: www.soda-pro.com/soda-products/ai-forecast

[23] B. Espinar *et al.*, "Helioclim-3: a near-real time and long-term surface solar irradiance database," in *Workshop on" Remote Sensing Measurements for Renewable Energy"*, 2012.

[24] M. Lefevre *et al.*, "Mcclear: a new model estimating downwelling solar radiation at ground level in clear-sky conditions," *Atmospheric Measurement Techniques*, vol. 6, no. 9, pp. 2403–2418, 2013.

[25] W. Holmgren, C. Hansen, and M. Mikofski, "pvlib python: A python package for modeling solar energy systems," *Journal of Open Source Software*, vol. 3, no. 29, p. 884, 2018.

[26] E. Stai et al., "Dispatching stochastic heterogeneous resources accounting for grid and battery losses," *IEEE Trans. on Smart Grid*, vol. 9, no. 6, pp. 6522–6539, 2018.

[27] L. Zanni *et al.*, "Pmu-based linear state estimation of lausanne subtransmission network: Experimental validation," *EPSR*, vol. 189, p. 106649, 2020.

2 Achievement of deliverable

2.1 Date

March 2022

2.2 Demonstration of the deliverable

This deliverable has been achieved through:

- the development of a dedicated optimal control and scheduling framework;
- the development of two-layer model predictive control schems using short-term intra-day forecasts of the uncontrollable power injections;
- the validation of the proposed methodologies in a full-scale real environment via the REeL demonstrator site in Aigle, Switzerland.

3 Impact

This deliverables represent the final outcome of a series of activities undertaken in the frame of ReEL. This involves the development of the OPF-based control methodology, a PMU-based real-time grid state monitoring and a short-term PV forecasting, all patented, as well as the demonstration of those solutions in the real-grid of Aigle.

References

[1] R. Gupta, A. Zecchino, J.-H. Yi, and M. Paolone, "Reliable dispatch of active distribution networks via a two-layer grid-aware model predictive control," *Under review for the publication in the IEEE Open Access Journal of Power and Energy*, 2022.